Optical Properties of Energetic Materials: RDX, HMX, AP, NC/NG, and HTPB

R. A. Isbell and M. Q. Brewster

Department of Mechanical and Industrial Engineering, University of Illinois, Urbana, Illinois 61801 (USA)

Optische Eigenschaften von energetischen Materialien: RDX, HMX, AP, NC/NG, und HTPB

Die optischen Eigenschaften von RDX, HMX, AP, HTPB/IPDI-Binder und einem stabilisatorhaltigen NC/NG-Treibladungspulver (N5) wurden erhalten mittels FTIR-Transmissionsspektometrie im Bereich zwischen 2,5 μm und 18 μm. Für die kristallinen Materialien wurde die streuungskorrigierte KBr/Preßling-Methodik verwendet. Der Absorptionsindex (k) wurde direkt gemessen und der Brechungsindex (n) wurde abgeleitet unter Verwendung der Dispersionstheorie. Bei 10.600 μm wurden folgende Absorptionskoeffizienten erhalten: AP, 190 cm^{-1} (bei 10.6036 μm 240 cm^{-1}); HTPB/IPDI, 360 cm^{-1}; N5, 510 cm^{-1}; RDX, 2800 cm^{-1}; und HMX, 5670 cm^{-1}.

Propriétés optiques de matériaux énergétiques: RDX, HMX, AP, NC/NG, et HTPB

On a obtenu les propriétés optiques de RDX, HMX, AP, HTPB/IPDI et d'une poudre propulsive NC/NG à base de stabilisant (N5) au moyen de la spectrométrie à transmission FTIR entre 2,5 μm et 18 μm. Pour les matériaux cristallins, on a utilisé la méthodologie des comprimés de KBr à dispersion corrigée. L'indice d'absorption (k) a été mesuré directement et l'indice de réfraction (n) a été déduit en utilisant la théorie de dispersion. A 10,600 μm, on a obtenu les coefficients d'extinction suivants: AP, 190 cm^{-1} (à 10,6036 μm 240 cm^{-1}); HTPB/IPDI, 360 cm^{-1}; N5, 510 cm^{-1}; RDX, 2800 cm^{-1}; et HMX, 5670 cm^{-1}.

Summary

Optical properties of RDX, HMX, AP, HTPB/IPDI and a catalyzed NC/NG propellant (N5) were obtained from 2.5 μm to 18 μm using FTIR transmission spectrometry. Scattering-corrected KBr pellet methodology was used for the crystalline materials. Absorption index (k) was measured directly and refractive index (n) was deduced using dispersion theory. At 10.600 μm the absorption coefficients were AP, 190 cm^{-1} (240 cm^{-1} at 10.6036 μm); HTPB/IPDI, 360 cm^{-1}; N5, 510 cm^{-1}; RDX, 2800 cm^{-1}; and HMX, 5670 cm^{-1}.

1. Introduction

Optical properties of energetic materials are of interest for a variety of reasons. Infrared transmission spectra are commonly used to identify chemical structure by correlating absorption peaks with certain bonds and lattice vibrations. For these purposes qualitative (or relative) information about absorption strength as obtained from conventional FTIR spectroscopy is sufficient. Other studies require quantitative (or absolute) optical property information, *i.e.*, the optical constants, n (refractive index) and k (absorption index). Investigative methods that are benefited by knowledge of the material optical constants include laser pyrolysis, for determining energetic material decomposition chemistry, and laser-augmented combustion and ignition. Knowledge of the optical constants allows estimation of surface (Fresnel) reflection losses and spatial distribution of radiation absorption. While reports containing relative absorbance are plentiful, optical constant data for energetic materials are scarce.

This paper reports the results of a technique developed to determine optical constants for energetic materials. Data are reported for AP, RDX, HMX, HTPB/IPDI binder, and a catalyzed double base propellant, N5. The method uses KBr pellet-FTIR transmission spectrometry in conjunction with dispersion theory. This paper emphasizes the results obtained; the technique itself is discussed in more detail in Ref. 1. The method accounts for radiation scattered by the KBr pellets. The results at 10.6 μm were checked by an independent technique using a CO_2 laser and spatial filtering to remove scattered radiation. Advantages of the FTIR/KBr-pellet method are that optical constants can be obtained even in strongly absorbing regions with sufficient dilution and fine enough particles and they can be obtained over a broad spectral range.

2. Procedure and Analysis

AP, RDX, and HMX samples were prepared by dispersing their respective powders in KBr powder and pressing the mixture into pellets. Before mixing, both energetic material and KBr powders were ground until most of the particles were submicron in size. Binder samples were formed by pressing uncured binder between plexiglass strips and curing them into thin sheets. N5 samples were formed by slicing into thin sections with a microtome. Transmission spectra were measured for samples with various optical thickness using an FTIR spectrometer over the range of 2.5 μm to 18 μm. The AP came coated with tricalcium phosphate (TCP), an anticaking agent; its effect on optical properties was negligible at most wavelengths. The RDX and HMX contained only trace amounts of impurities which did not affect the optical properties. The binder was a mixture of 84% mass fraction HTPB, 6% isophorone diisocyanate (IPDI), and 10% dioctyl acetate (DOA), N5 consists of 50% nitrocellulose (NC), 34.9% nitroglycerin (NG), 2% 2-nitrodiphenylamine, 10.5% diethylphthalate (DEP), 1.2% H-101 lead octoate, 1.2% S-202 lead salicylate, and 0.2% candelilla wax. Optical properties

 0721-3115/98/0408–0218 $17.50+.50/0

were determined by measuring the normal, spectral transmissivity of the samples. In the case of KBr pellets, KBr was taken to be non-absorbing in the spectral range of interest, although scattering by KBr was accounted for as described in Ref. 1. The KBr pellet transmissivity data were analyzed in the Rayleigh-Gans limit of light scattering and absorption by small particles. The optical properties reported here include the optical constants, n (refractive index) and k (absorption index), the absorption coefficient,

$$K_a = \frac{4\pi k}{\lambda_o} \tag{1}$$

where λ_0 is the vacuum ($\sim$ air) wavelength of the incident intensity, and the normal Fresnel interface reflectance,

$$R_n = \frac{(n-1)^2 + k^2}{(n+1)^2 + k^2}. \tag{2}$$

The measured spectra for absorption index $k(\lambda)$, were curve fit using an optimization routine and dispersion theory relations[2].

$$n^2 - k^2 = n_e^2 + \sum_j \frac{\omega_{p,j}^2\left(\omega_{o,j}^2 - \omega^2\right)}{\left(\omega_{o,j}^2 - \omega^2\right)^2 + \gamma_j^2\omega^2} \tag{3}$$

$$2nk = \sum_j \frac{\omega_{p,j}^2\gamma_j\omega}{\left(\omega_{o,j}^2 - \omega^2\right)^2 + \gamma_j^2\omega^2} \tag{4}$$

Here ω_p, ω_0, and γ represent the oscillator strength (plasma frequency), oscillator frequency, and line width of the "j$^{\text{th}}$" oscillator, respectively. The residual value of refractive index n_e occurs at the short wavelength end of the spectral interval of interest, which is the visible/near infrared region in this case. Its value results from electronic transitions in the ultraviolet region. This procedure resulted in values for the oscillator parameters (ω_p, ω_o, and γ) and the refractive index spectrum $n(\lambda)$. These parameters allow one to calculate n and k at any wavelength of interest using Eqs. (3) and (4).

3. Results

Figure 1 shows the absorption coefficient spectra, $K_{a,\lambda}$, for each of the materials investigated. The spectra are active over various regions corresponding to the molecular or lattice structures of the individual materials. The HTPB/IPDI binder exhibits a relatively low absorption coefficient with extended activity over a broad spectral range, typical of polymeric materials with many covalent bonds. At the other extreme, AP exhibits a relatively high absorption coefficient over a relatively few, narrow bands, typical of ionic salts. The behavior of N5, RDX, and HMX falls between these extremes with intermediate absorption coefficient values spread over a moderate spectral range. Some of the peaks in $K_{a,\lambda}$ are truncated due to insufficient transmission at these wavelengths. At 10.600 μm the

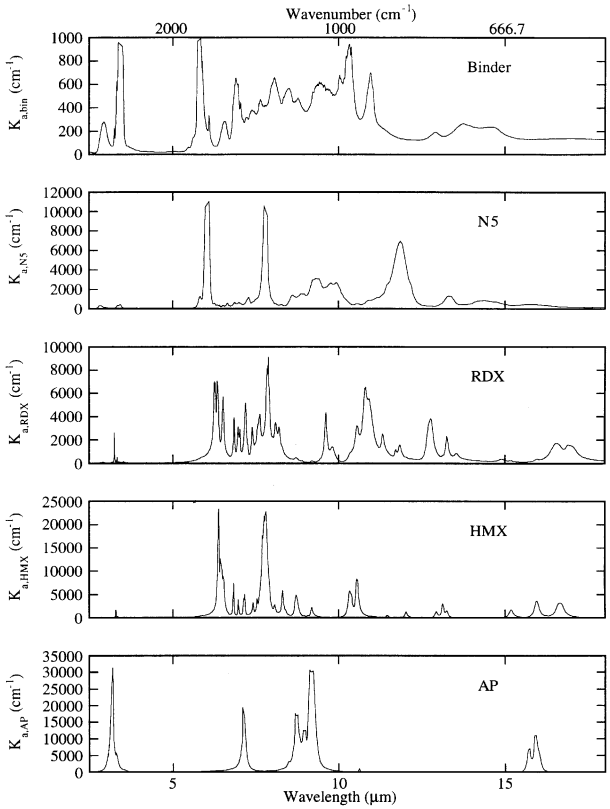

Figure 1. Absorption coefficient spectra for HTPB binder, N5, RDX, HMX, and AP.

absorption coefficients are $K_{a,AP} = 191$ cm^{-1}, $K_{a,RDX} = 2803$ cm^{-1}, $K_{a,HMX} = 5672$ cm^{-1}, $K_{a,bin} = 317$ cm^{-1}, and $K_{a,N5} = 511$ cm^{-1}.

The absorption index (k) is calculated from $K_{a,\lambda}$ using Eq. (1) and the results are shown in Fig. 2. AP has the simplest spectral structure of the materials tested. It has strong ionic bonding and its absorption spectrum manifests a few, widely spaced, strong bands with k values generally of order one. Absorption peaks occur at 3.19, 7.14, 8.49, 8.73, 8.98, 9.20, 10.63, 15.72, and 15.97 μm. These peaks reveal the structure and bonding present in AP. The bands at 3.19 μm and 7.14 μm are fundamental frequencies of the ammonium ion in the infrared region[3]. The peak at 3.19 μm is strong and broad and corresponds to N-H stretching. The peak at 7.14 μm is narrow but very strong and corresponds to NH_4^+ deformation. The bands in the range 8.49 μm to 9.20 μm overlap forming the strongest absorption region which corresponds to distortion of the tetrahedral ClO_4^- ion[4]. Another group of strong, narrow bands overlap at 15.72 μm and 15.97 μm. These bands give structure to the degenerate frequencies of the perchlorate ion displayed in dilute solution[5]. Another very weak peak occurs at 10.63 μm and corresponds to the "breathing" frequency of the perchlorate ion[6].

RDX (Fig. 2) has a more complicated molecular structure than AP as indicated by numerous, closely spaced bands ($k \sim O(10^{-1})$). These bands exhibit some overlap and are moderately strong but have maximum k values somewhat less than those for AP. The value of k_{RDX} approaches 0.6

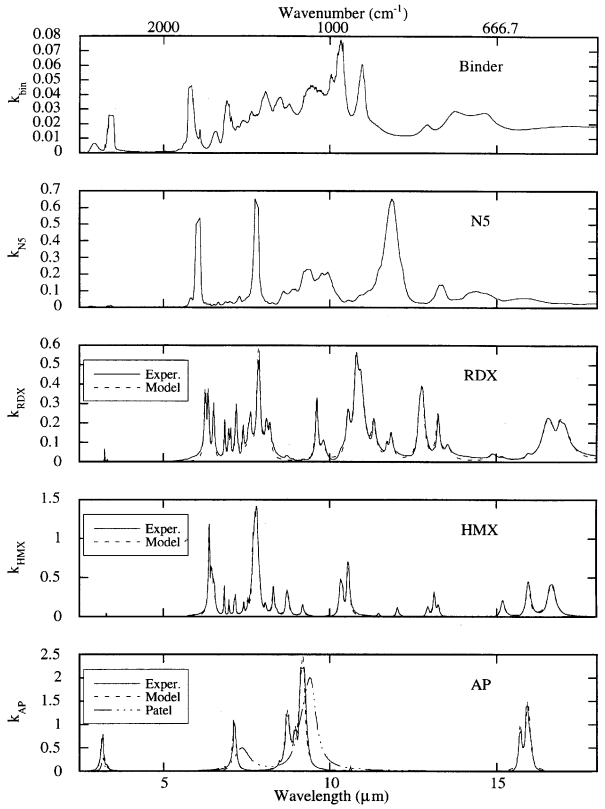

Figure 2. Absorption index spectra for HTPB binder, N5, RDX, HMX, and AP.

near 7.8 μm and 10.8 μm. The complex spectrum arises from a complex molecular structure consisting of potentially 21 bond stretches, 36 bond-angle bends, 3 wag-angle bends, and 9 Leonard-Jones non-bonded interactions. CH participates over 2700 to 3100 and 0 to 300 cm^{-1}. No other bonds contribute appreciably to these regions. The CN bond has many bands over 400 to 1600 cm^{-1}. NO participates strongly over 1500 to 1600 cm^{-1} with weaker peaks over 500 to 1300 cm^{-1}. N-C-N bending contributes weakly over 350 to 843 cm^{-1}. H-C-H bending has a strong peak at 1234 cm^{-1} with weaker bands over 1039 to 1311 cm^{-1}[7]. HMX has a structure similar to that of RDX ($k \sim O(10^{-1})$) with numerous, closely-spaced, moderately strong bands. The value of k_{HMX} approaches 1.4 at 7.88 μm. HMX bonds participate in similar spectral regions as in RDX but the spectra show shifted peak positions and strengths.

The binder is a polymeric mixture of materials with an even more complex molecular structure characterized by prevalent covalent bonding. The spectrum for k_{bin} (Fig. 2) shows much overlap of numerous weak bands ($k \sim O(10^{-2})$) that participate over most of the spectrum with maximum values approaching 0.08 near 10.4 μm. Several peaks in the spectrum result from curing bonds between the NCO groups of IPDI and the OH groups of HTPB. Others are due to HTPB cross-linking and cyclization[8]. Strong peaks at 5.78 μm and 5.90 μm correspond to intermolecular hydrogen-bonded C═O stretching. The peak at 5.90 μm is characteristic of α,β-unsaturated carbonyl groups. A peak at 2.95 μm is characteristic of OH. Peaks at 6.57 μm and 14.62 μm correspond to N-H in-plane and out-of-plane bending[9]. A peak at 8.08 μm corresponds to C-O stretching[10]. For HTPB, ═CH stretching occurs at 3.25 μm and 3.33 μm and C═C stretching occurs at 6.10 μm. Alkane C-H stretching occurs at 3.44 μm and 3.52 μm. Alkane C-H deformation occurs at 6.94 μm. The alkene ═CH deformation vibrations occur at 13.76 μm (cis R-CH═CH-R), 10.99 μm and 10.06 μm (1,2-vinyl ═CH), and 10.38 μm (trans R-CH═CH-R)[8].

The infrared spectrum of N5 (Fig. 2) corresponds to that of its primary constituents NC and NG. It exhibits many weak bands with much overlap and some relatively strong bands ($k \sim O(10^{-1})$) with values for k_{N5} approaching 0.6 near 6 μm and 0.7 near 7.8 μm and 11.9 μm. Since NC and NG are the primary constituents and have similar structure, these bands are suspected to have fine structure (which is missed due to truncation) and are attributed to bonds present in the NC and NG makeup. Studies identifying and attributing these peaks to particular bonds were not found.

For further reference, detailed discussions of molecular structure and bond-peak assignments are available for AP[3-6], RDX[7,11], and HTPB[8-10].

Figure 3 shows the k-spectra for each material in the vicinity of 10.6 μm. Clearly, the absorption indices for the binder and for N5 change very little in this spectral region. The absorption indices for RDX and HMX vary somewhat over 10.4 μm–10.8 μm, but not so steeply in the immediate vicinity of 10.6 μm as is the case for AP. A weak resonance at 10.63 μm in the AP spectrum corresponding to the perchlorate ion breathing frequency[6], gives rise to a rapid change in the absorption index of AP near 10.6 μm. In fact, k_{AP} (as well as $K_{a,AP}$) changes an order of magnitude over 0.03 μm. At this wavelength (10.6 μm) the absorption index values are $k_{AP} = 0.016$, $k_{RDX} = 0.236$, $k_{HMX} = 0.478$, $k_{bin} = 0.027$, and $k_{N5} = 0.043$.

The effect of spectral resolution in the FTIR measurements was also considered. Most measurements were con-

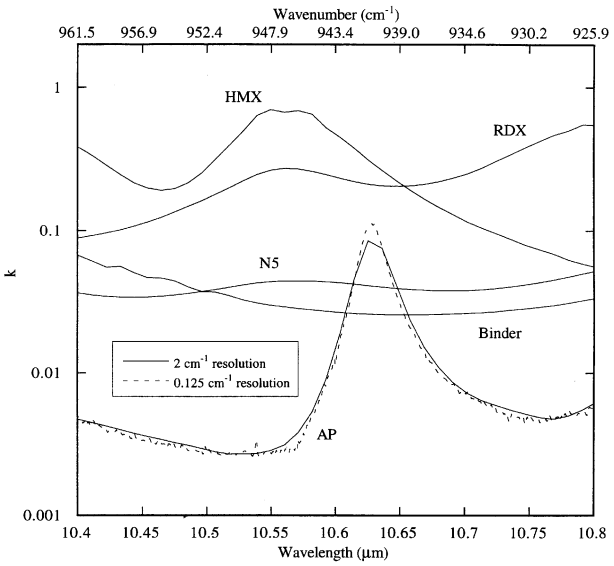

Figure 3. Absorption index spectra for HTPB binder, N5, RDX, HMX, and AP near 10.6 μm.

ducted with a resolution of $2\,cm^{-1}$. To check this effect, relative absorbance spectra for each material were also measured at $0.125\,cm^{-1}$ (0.0028 μm at 10.6 μm) resolution over the spectral range 1000–900 cm^{-1} (10.0–11.1 μm). Only AP showed a noticeable difference. The $0.125\,cm^{-1}$ resolution absorbance spectrum for AP (Fig. 3) showed slightly better definition in the perchlorate ion breathing frequency peak at 10.63 μm than the $2\,cm^{-1}$ resolution spectrum. Absorption increased at the band center and decreased in the wings for the higher resolution spectrum; the reduction was 12% at 10.6 μm. Except for refinement of the peak at 10.63 μm and more pronounced noise, no new spectral features were revealed. Peak refinement was not apparent for RDX, HMX, binder, and N5 near 10.6 μm since their bands in this region are not as narrow as the 10.63 μm peak for AP.

To determine the refractive index (n), dispersion theory was applied to the measured absorption index spectra for RDX, HMX, and AP. Refractive index values in the visible region were assumed as follows: $n_{e,AP} = 1.484$, $n_{e,RDX} = 1.597$, $n_{e,HMX} = 1.594$. A value for n_e was unavailable for the binder and N5. The absorption index was modeled by varying the oscillator parameters of Eqs. (3) and (4). AP was modeled with 9 oscillators, RDX with 40, and HMX with 39. Tables 1, 2, and 3 show the oscillator parameters for AP, RDX, and HMX, respectively. The Lorentzian-modeled k-spectra are shown in Fig. 2 with the experimentally determined values. Generally good agreement with the experimental spectra demonstrates the appropriateness of the Lorentzian model. The refractive index and normal reflectance, n and R_n, were calculated with the oscillator parameters in Tables 1, 2, and 3, and Eqs. (2), (3) and (4). Figures 4 and 5 show the refractive index and normal reflectivity spectra for RDX, HMX, and AP. For AP, the bands near 9 μm are very strong and result in reflectance approaching 50% in this spectral region. For comparison, measurements of the near normal reflectance[12] of pressed AP pellets are also shown in Fig. 5. The values inferred in the present study from FTIR/KBr pellet transmission agree well with the AP pellet reflectivity measurements, considering that the spectral resolution of the reflectivity measurements (using a grating monochromator) was not as good and did not extend beyond 10 μm. It also appears that there might have been a spectral calibration error in the measured reflectivities. The reflectivity for RDX fluctuates rapidly throughout the spectrum with values ranging from 2% to 11%. For HMX, strong bands near 6.4 μm and 7.75 μm result in reflectances varying from near zero to 23% and 28%, respectively. At 10.6 μm, $R_{n,AP} = 7.46\%$, $R_{n,RDX} = 4.70\%$, and $R_{n,HMX} = 15.0\%$.

Since large reflectivity is generally associated with strong absorption (large k) for n of order one, it may seem paradoxical that RDX has a stronger absorption index (0.236 versus 0.016) but a weaker reflectivity (4.6% versus 7.5%) than AP at 10.6 μm. However, for AP, 10.6 μm is in the high wavelength wing of a very strong resonance ($k_{AP,\max} \sim 2.5$) and in the low wavelength wing of a weak resonance ($k_{AP,\max} \sim 0.1$). The weak resonance does not strongly depress $R_{n,AP}$. On the other hand,. for RDX, 10.6 μm is in the high wavelength wing of a relatively weak resonance ($k_{RDX,\max} \sim 0.3$) and in the low wavelength wing of a relatively strong resonance ($k_{RDX,\max} \sim 0.6$). The combined effect depresses $R_{n,RDX}$ to near 3% around 10.5 μm before elevating it to near 11% around 11 μm. Strong resonances can extend their effects to wide regions in frequency space. The spacing and strength of adjacent bands can have unexpected effects on R_n.

Table 1. Oscillator Parameters for AP

Oscillator	ω_0 (1/s)	γ (1/s)	ω_p (1/s)
1	$5.890(10^{14})$	$1.785(10^{13})$	$1.634(10^{14})$
2	$2.628(10^{14})$	$3.569(10^{12})$	$5.636(10^{13})$
3	$2.213(10^{14})$	$1.315(10^{12})$	$7.515(10^{12})$
4	$2.142(10^{14})$	$2.818(10^{12})$	$4.415(10^{13})$
5	$2.095(10^{14})$	$1.691(10^{12})$	$2.067(10^{13})$
6	$2.036(10^{14})$	$2.912(10^{12})$	$8.642(10^{13})$
7	$1.768(10^{14})$	$5.636(10^{11})$	$6.200(10^{12})$
8	$1.195(10^{14})$	$6.387(10^{11})$	$1.371(10^{13})$
9	$1.177(10^{14})$	$9.393(10^{11})$	$2.630(10^{13})$

Table 2. Oscillator parameters, for RDX

Oscillator	ω_0 (1/s)	γ(1/s)	ω_p (1/s)
1	$5.777(10^{14})$	$1.240(10^{12})$	$1.353(10^{13})$
2	$5.759(10^{14})$	$1.184(10^{12})$	$1.165(10^{13})$
3	$5.638(10^{14})$	$2.254(10^{12})$	$7.890(10^{12})$
4	$2.996(10^{14})$	$4.020(10^{12})$	$3.391(10^{13})$
5	$2.957(10^{14})$	$2.987(10^{12})$	$2.955(10^{13})$
6	$2.891(10^{14})$	$2.367(10^{12})$	$1.324(10^{13})$
7	$2.880(10^{14})$	$2.198(10^{12})$	$2.236(10^{13})$
8	$2.742(10^{14})$	$1.879(10^{12})$	$1.785(10^{13})$
9	$2.695(10^{14})$	$1.550(10^{12})$	$1.371(10^{13})$
10	$2.673(10^{14})$	$1.484(10^{12})$	$1.334(10^{13})$
11	$2.610(10^{14})$	$2.330(10^{12})$	$2.330(10^{13})$
12	$2.585(10^{14})$	$1.315(10^{12})$	$4.997(10^{12})$
13	$2.539(10^{14})$	$2.104(10^{12})$	$1.606(10^{13})$
14	$2.485(10^{14})$	$3.043(10^{12})$	$1.550(10^{13})$
15	$2.463(10^{14})$	$2.630(10^{12})$	$1.916(10^{13})$
16	$2.387(10^{14})$	$3.645(10^{12})$	$4.039(10^{13})$
17	$2.345(10^{14})$	$1.785(10^{12})$	$5.486(10^{12})$
18	$2.319(10^{14})$	$2.630(10^{12})$	$1.803(10^{13})$
19	$2.289(10^{14})$	$2.874(10^{12})$	$1.935(10^{13})$
20	$1.953(10^{14})$	$1.879(10^{12})$	$1.935(10^{13})$
21	$1.913(10^{14})$	$2.442(10^{12})$	$1.165(10^{13})$
22	$1.779(10^{14})$	$2.198(10^{12})$	$1.493(10^{13})$
23	$1.738(10^{14})$	$2.311(10^{12})$	$2.080(10^{13})$
24	$1.716(10^{14})$	$3.908(10^{12})$	$3.047(10^{13})$
25	$1.657(10^{14})$	$2.198(10^{12})$	$1.527(10^{13})$
26	$1.602(10^{14})$	$1.277(10^{12})$	$5.899(10^{12})$
27	$1.585(10^{14})$	$1.973(10^{12})$	$1.184(10^{13})$
28	$1.478(10^{14})$	$1.804(10^{12})$	$1.172(10^{13})$
29	$1.469(10^{14})$	$1.785(10^{12})$	$1.659(10^{13})$
30	$1.417(10^{14})$	$1.390(10^{12})$	$1.240(10^{13})$
31	$1.388(10^{14})$	$2.686(10^{12})$	$9.506(10^{12})$
32	$1.261(10^{14})$	$2.142(10^{12})$	$5.504(10^{12})$
33	$1.237(10^{14})$	$1.597(10^{12})$	$2.818(10^{12})$
34	$1.177(10^{14})$	$1.033(10^{12})$	$2.499(10^{12})$
35	$1.135(10^{14})$	$2.593(10^{12})$	$1.326(10^{13})$
36	$1.112(10^{14})$	$1.841(10^{12})$	$6.481(10^{12})$
37	$1.103(10^{14})$	$3.363(10^{12})$	$1.370(10^{13})$
38	$9.133(10^{13})$	$5.354(10^{12})$	$1.069(10^{13})$
39	$8.658(10^{13})$	$3.137(10^{12})$	$1.091(10^{13})$
40	$7.719(10^{13})$	$2.367(10^{12})$	$8.510(10^{12})$

Table 3. Oscillator parameters for HMX

Oscillator	ω_0 (1/s)	γ (1/s)	ω_p (1/s)
1	$6.814(10^{14})$	$1.963(10^{13})$	$6.012(10^{12})$
2	$6.479(10^{14})$	$3.607(10^{13})$	$1.443(10^{13})$
3	$5.705(10^{14})$	$1.371(10^{12})$	$3.475(10^{12})$
4	$5.686(10^{14})$	$8.078(10^{11})$	$1.522(10^{13})$
5	$5.623(10^{14})$	$2.686(10^{12})$	$4.885(10^{12})$
6	$5.604(10^{14})$	$2.123(10^{12})$	$3.043(10^{12})$
7	$5.470(10^{14})$	$2.198(10^{12})$	$2.292(10^{12})$
8	$5.303(10^{14})$	$1.044(10^{13})$	$7.515(10^{12})$
9	$5.198(10^{14})$	$3.832(10^{12})$	$3.288(10^{12})$
10	$2.942(10^{14})$	$1.634(10^{12})$	$3.756(10^{13})$
11	$2.904(10^{14})$	$5.448(10^{12})$	$5.504(10^{13})$
12	$2.876(10^{14})$	$1.450(10^{12})$	$1.854(10^{13})$
13	$2.748(10^{14})$	$1.108(10^{12})$	$1.948(10^{13})$
14	$2.692(10^{14})$	$1.058(10^{12})$	$1.321(10^{13})$
15	$2.633(10^{14})$	$9.769(10^{11})$	$1.016(10^{13})$
16	$2.620(10^{14})$	$1.443(10^{12})$	$1.715(10^{13})$
17	$2.532(10^{14})$	$1.277(10^{12})$	$1.127(10^{13})$
18	$2.491(10^{14})$	$1.503(10^{12})$	$1.161(10^{13})$
19	$2.437(10^{14})$	$1.935(10^{12})$	$2.367(10^{13})$
20	$2.420(10^{14})$	$1.653(10^{12})$	$2.442(10^{13})$
21	$2.402(10^{14})$	$2.611(10^{12})$	$5.486(10^{13})$
22	$2.384(10^{14})$	$3.194(10^{12})$	$3.382(10^{13})$
23	$2.327(10^{14})$	$2.198(10^{12})$	$1.428(10^{13})$
24	$2.260(10^{14})$	$1.973(10^{12})$	$2.442(10^{13})$
25	$2.152(10^{14})$	$2.442(10^{12})$	$2.499(10^{13})$
26	$2.043(10^{14})$	$1.879(10^{12})$	$1.409(10^{13})$
27	$1.817(10^{14})$	$1.422(10^{12})$	$1.800(10^{13})$
28	$1.806(10^{14})$	$9.581(10^{11})$	$1.172(10^{13})$
29	$1.777(10^{14})$	$1.576(10^{12})$	$2.698(10^{13})$
30	$1.637(10^{14})$	$9.393(10^{11})$	$4.509(10^{12})$
31	$1.560(10^{14})$	$9.168(10^{11})$	$7.665(10^{12})$
32	$1.451(10^{14})$	$9.769(10^{11})$	$7.263(10^{12})$
33	$1.429(10^{14})$	$8.736(10^{11})$	$1.116(10^{13})$
34	$1.416(10^{14})$	$7.740(10^{11})$	$7.045(10^{12})$
35	$1.237(10^{14})$	$1.044(10^{12})$	$9.356(10^{12})$
36	$1.178(10^{14})$	$9.393(10^{11})$	$1.281(10^{13})$
37	$1.128(10^{14})$	$1.841(10^{12})$	$1.741(10^{13})$
38	$8.229(10^{13})$	$1.161(10^{12})$	$7.609(10^{12})$
39	$7.834(10^{13})$	$1.264(10^{12})$	$5.185(10^{12})$

The normal reflectivities at 10.6 μm for N5 and binder were calculated from the absorbance intercepts (extrapolation of measured absorbance versus sample thickness to zero thickness). For N5, the calculated value $R_{n,N5} = 3.58\%$ seems reasonable. The corresponding refractive index from Eq. (2) is $n_{N5} = 1.46$. For the binder, the absorbance intercept corresponds to $R_{n,bin} = 35.49\%$. Since this value seemed too high a similar analysis was repeated for a binder mixture of HTPB : IPDI = 90 : 10 (no DOA added) with a reduced spectrometer aperture setting, giving $K_{a,bin} = 333\ \text{cm}^{-1}$, $k_{bin} = 0.028$, and $R_{n,bin} = 33.76\%$. (Samples without DOA could only be prepared to a minimum thickness twice that of samples with DOA.) Although the results without DOA were very close to those obtained for the binder mixture with DOA, a normal reflectivity of 35% still seemed unrealistically high (it would require a refractive index of either 0.25 or 3.9 according to Eq. 2). The cause of the erroneously high indicated normal reflectance for the binder material was ultimately determined to be sample uniformity. Relatively thick binder samples are probably isotropic with random

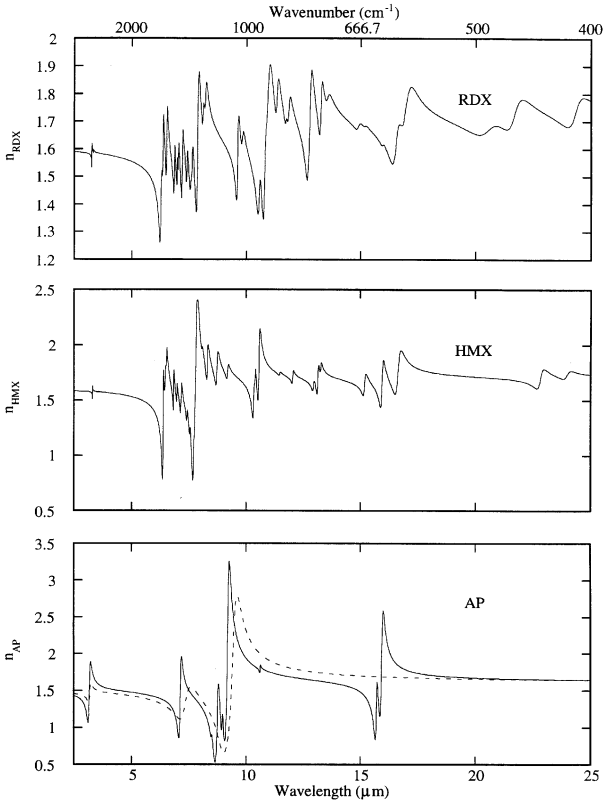

Figure 4. Refractive index for RDX, HMX, and AP from dispersion theory (dashed line from Ref. 12).

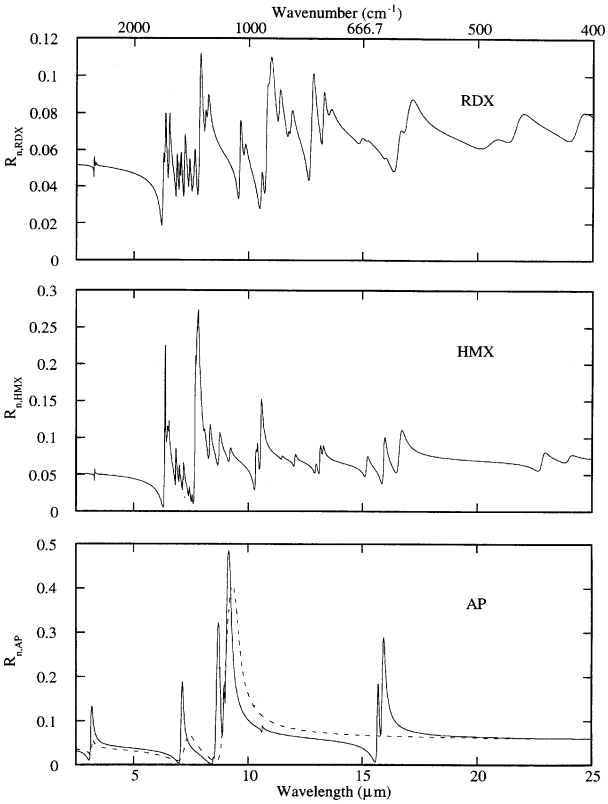

Figure 5. Normal reflectivity for RDX, HMX, and AP from dispersion theory (dashed line from Red. 12).

polymer chain orientations. However, thinner samples are probably anisotropic with preferential lateral orientation of polymer chains due to pressing the samples to thicknesses on the order of the polymer chain length. This results in increased absorbances for thinner samples and a higher absorbance intercept (and R_n). As a result $K_{a,bin}$ and k_{bin} determined in this manner would be underpredicted and dependent on the range of sample thickness investigated. The effect will be smaller for the thicker samples. Other factors contributing to the indicated reflectivity error are sample compression and regression slope uncertainty. Compression of samples during thickness measurement due to a low modulus would also result in a higher intercept. Such deformation would not occur for the KBr pellets or N5 samples since they are not as flexible. Small errors in slope from the regression analysis can also lead to considerable error in the calculated reflectance with only minimal error in the absorption coefficient. Accordingly, it is believed that the absorbance intercept overpredicts $R_{n,bin}$. To obtain more accurate measurements for the binder, near normal specular reflectance measurements were made for 1 cm thick binder samples at 10.6 μm yielding $R_{\theta=28^\circ,bin} = 7.18\%$. With k and R_n values known at 10.6 μm, Eq. (2) yields $n_{bin} = 1.73$. Alternatively, a linear fit of absorbance data for the thickest binder samples which is forced through the absorbance intercept corresponding to the measured reflectance results in $K_{a,bin} = 361\ \text{cm}^{-1}$, $k_{bin} = 0.030$, and $n_{bin} = 1.73$. These values are probably more representative of the bulk, isotropic binder mixture than those deduced for the thin, transmissive samples, as discussed above.

4. Discussion

Both the FTIR and laser-spatial filtering KBr pellet techniques used in this study are dependent on the assumption of Rayleigh-Gans scattering to obtain accurate absorption coefficient data for crystalline materials. If the conditions for Rayleigh-Gans scattering are not satisfied but the data are analyzed under that assumption the absorption coefficient K_a will be underpredicted. The key condition that must be satisfied is that the particles be optically thin $K_a d \ll 1$ where d is particle diameter. In this study particles were ground to the sub micron size range, as verified by optical microscopy, but no attempt at a more accurate size determination was made. Assuming an effective average absorbing particle size of 0.5 μm and using 0.3 as the maximum limit of $K_a d$ gives a maximum absorption coefficient of $6000\ \text{cm}^{-1}$. Thus, there is high confidence in the accuracy of the indicated absorption coefficients below this value and an increasing (although as yet unquantified) tendency for underestimation in the values reported above $6000\ \text{cm}^{-1}$. Except for the highest absorption peaks, most of the values for HMX and RDX were under this value, including those at 10.6 μm. At this wavelength, the absorption coefficients for HMX and RDX were $5670\ \text{cm}^{-1}$ and $2800\ \text{cm}^{-1}$, respectively. Ostmark et al.[13], reported an absorption coefficient of $875\ \text{cm}^{-1}$ at 10.6 μm for RDX but did not report particle size. This discrepancy for RDX (2800 versus $875\ \text{cm}^{-1}$) would be consistent with the systematic error that would occur if large (say, $d > 3\ \mu m$) RDX particles were used for which $K_a d > 1$ but the data were interpreted assuming the apparent pellet absorption coefficient was the intrinsic RDX absorption coefficient times the RDX particle volume fraction (*i.e.*, Rayleigh-Gans limit).

For AP, the indicated absorption coefficient typically exceeded $6000\ \text{cm}^{-1}$ in the absorption bands and therefore further measurements should be conducted to better quantify the potential error in the AP measurements in the band regions. Near 10.6 μm, however, where the laser-spatial filtering technique was used with AP to confirm the FTIR measurements, the absorption coefficient of AP ($190\ \text{cm}^{-1}$) was well below the $6000\ \text{cm}^{-1}$ threshold value.

5. Conclusion

The FTIR/KBr-pellet transmission spectroscopy technique has been developed to obtain the optical constants of relatively strongly absorbing energetic materials, such as HMX, RDX, and AP over the range 2.5 μm to 25 μm. A laser-spatial filtering technique was also developed and used with AP to verify the FTIR approach. Absorption coefficient and absorption index were measured directly in the Rayleigh-Gans scattering limit and refractive index was determined from dispersion theory. FTIR measurements were also conducted on homogeneous binder (HTPB/IPDI) and double base propellant (N5) samples. Generally good results were obtained. However, polymer chain orientation effects (anisotropic optical properties) were noticed with the thinnest binder samples. Table 4 summarizes the optical properties measured for bulk, isotropic material at 10.6 μm.

Table 4. Optical Properties at 10.600 μm

Material	K_a (cm^{-1})	k	n	R_n (%)
AP	191 (239)[a]	0.016 (0.020)[a]	1.75	7.46
RDX	2803	0.236	1.49	4.70
HMX	5672	0.478	2.14	15.0
binder[(b)]	361	0.030	1.73	7.18
N5	511	0.043	1.46	3.58

[(a)]at 10.6036 μm.
[(b)]for random polymer orientation.

6. References

(1) R. A. Isbell, and M. Q. Brewster, "*Optical Properties of Energetic Materials from Infrared Spectroscopy*," *J. Thermophys. Heat Transfer 11*, 65–71 (1997).
(2) M. Q. Brewster, "*Thermal Radiative Transfer and Properties*", John Wiley & Sons, New York 1992, p. 162.
(3) T. C. Waddington, "Infrared Spectra, Structure, and Hydrogen-Bonding in Ammonium Salts," *J. Chemical Society Pt. IV*, 4340–4344 (1958).
(4) J. C. Petricciani, S. E. Wiberley, W. H. Bauer, and T. W. Clapper, "The Effects of a Chlorate Impurity on the Thermal Stability of Ammonium Perchlorate," *J. Physical Chemistry 64*, 1309–1311 (1960).
(5) G. Herzberg, "*Infrared and Raman Spectra of Polyatomic Molecules*". Van Nostrand, New York 1945, p. 167.
(6) S. D. Ross, "Forbidden Transitions in the Infrared Spectra of Some Tetrahedral Anions–I. Perchlorates," *Spectrochimica Acta 18*, 225–228 (1962).
(7) T. D. Sewell, C. C. Chambers, and D. L. Thompson, "Power Spectral Study of the Classical Vibrational Dynamics of RDX," *Chemical Physics Letters 208*, 125–134 (1993).
(8) J. K. Chen, S. S. Cheng, and S. C. Chou, "DSC, TG and Infrared Spectroscopic Studies of HTPB and Butacene Propellant Polymers," *AIAA Paper 94-3176* (1994).
(9) R. A. Nyquist, "Infrared Spectra-Structure Correlations of Carbamic Acid: Aryl-, Alkyl Esters," *Spectrochimica Acta 29A*, 1635–1641 (1973).
(10) James C. Carter, and Jorge E. Devia, "Vibrational Analysis of Methylcarbamate and N,N-Dichloromethylcarbamate," *Spectrochimica Acta 29A*, 623–632 (1973).
(11) J. Alix, and S. Collins, "The Photochemistry of RDX in Solid Argon at 10 K," *Canadian J. Chemistry 69*, 1535–1538 (1991).
(12) R. S. Patel, and M. Q. Brewster, "Optical Constants of Propellant-Grade Ammonium Perchlorate," *AIAA Journal 24*, 1878–1880 (1986).
(13) H. Ostmark, M. Carlson, and K. Ekvall, "Laser Ignition of Explosives: Effects of Laser Wavelength on the Threshold Ignition Energy," *J. Energetic Materials 12*, 63–83 (1994).

Acknowledgements

Support for this work from the Office of Naval Research (N00014-91-J-1977), N00014-97-1-0085). Richard S. Miller scientific officer, is gratefully acknowledged. The support of the Naval Air Warfare Center in providing RDX and HMX samples and communication with M. Nadler, P. Ashton, and J. Finlinson is also greatly appreciated. We are also indebted to Professor Richard O. Buckius and Jeff Ford of the University of Illinois for use of the FTIR spectrometer.

(Received April 3, 1997; Ms 20/97)